

Understanding Parton Distributions from Lattice QCD: Present Limitations and Future Promise *

J. W. Negele^a

^aCenter for Theoretical Physics, Massachusetts Institute of Technology,
77 Massachusetts Avenue, Cambridge, Massachusetts 02139, USA

This talk will explain how ground state matrix elements specifying moments of quark density and spin distributions in the nucleon have been calculated in full QCD, show how physical extrapolation to the chiral limit including the physics of the pion cloud resolves previous apparent conflicts with experiment, and describe the computational resources required for a definitive comparison with experiment.

1. INTRODUCTION

The focus of this workshop, the QCD structure of the nucleon, has two complementary aspects. One is measuring the quark and gluon structure experimentally. Decades of impressive high energy scattering experiments utilizing our knowledge of perturbative QCD and factorization have produced detailed knowledge of the light cone distributions of quarks and gluons in the nucleon, with the promise of even richer phenomenology to come. The second, and presently less well developed aspect, is calculating and understanding this quark and gluon structure theoretically, and the only method known at present to solve nonperturbative QCD is lattice field theory. Both aspects are essential, and I will show that the tools for quantitative calculation of nucleon structure are at hand, explain the scale of computational resources required for a definitive calculation, and argue that our field needs to provide these computational resources as well as experimental resources if we are to truly understand hadron structure.

Using the operator product expansion and lattice field theory, it is possible to calculate moments of quark distributions, and I will discuss here the first calculations in full QCD[1,2]. A major puzzle in the field has been the fact that quenched calculations of these moments, which ignore quark-antiquark excitations of the Dirac sea, disagree with experiment at the 20-50% level. I will show that contrary to earlier conjectures, at the quark masses accessible in practical calculations, including quark loops does not alter the results significantly. Rather, I will argue that the physical origin of the discrepancy with experiment has been incorrect extrapolation to the physical quark mass, and will show how extrapolation incorporating the leading non-analytic behavior required by chiral symmetry produces consistent results for the moments of quark distributions. In addition, we have also compared full QCD results with configurations that have been cooled

*Work supported in part by the U.S. Department of Energy (DOE) under cooperative research agreement #DE-FC02-94ER40818. MIT-CTP-3162

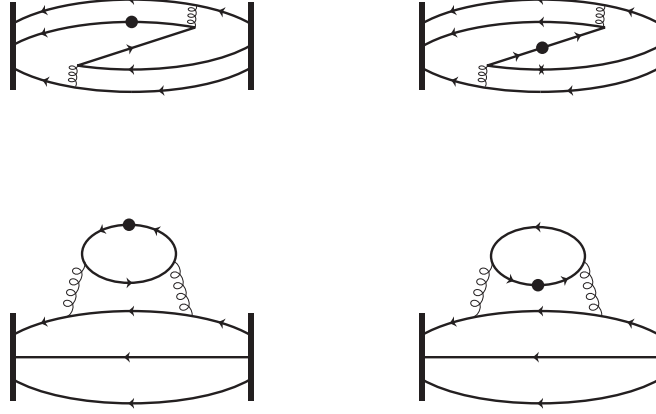


Figure 1. Connected (upper row) and disconnected (lower row) diagrams contributing to hadron matrix elements. The left column shows typical contributions of quarks and the right column shows contributions of antiquarks

to remove all the gluon contributions except for those of instantons and shown that the qualitative behavior of the moments is reproduced by the instanton content of the gluon configurations.

2. MOMENTS OF QUARK DISTRIBUTIONS IN THE PROTON

By the operator product expansion, moments of the following linear combinations of quark and antiquark distributions in the proton

$$\begin{aligned}
 \langle x^n \rangle_q &= \int_0^1 dx x^n (q(x) + (-1)^{n+1} \bar{q}(x)) \\
 \langle x^n \rangle_{\Delta q} &= \int_0^1 dx x^n (\Delta q(x) + (-1)^n \Delta \bar{q}(x)) \\
 \langle x^n \rangle_{\delta q} &= \int_0^1 dx x^n (\delta q(x) + (-1)^{n+1} \delta \bar{q}(x))
 \end{aligned} \tag{1}$$

are related to the following matrix elements of twist-2 operators

$$\begin{aligned}
 \langle PS | \bar{\psi} \gamma^{\{\mu_1} i D^{\mu_2} \dots i D^{\mu_n\} \psi | PS \rangle} &= 2 \langle x^{n-1} \rangle_q P^{\{\mu_1} \dots P^{\mu_n\}} \\
 \langle PS | \bar{\psi} \gamma^{\{\mu_1} \gamma_5 i D^{\mu_2} \dots i D^{\mu_n\} \psi | PS \rangle} &= 2 \langle x^{n-1} \rangle_{\Delta q} M S^{\{\mu_1} P^{\mu_2} \dots P^{\mu_n\}} \\
 \langle PS | \bar{\psi} \sigma^{[\alpha \{\mu_1} \gamma_5 i D^{\mu_2} \dots i D^{\mu_n\} \psi | PS \rangle} &= 2 \langle x^{n-1} \rangle_{\delta q} M S^{[\alpha} P^{\{\mu_1} P^{\mu_2} \dots P^{\mu_n\}}.
 \end{aligned} \tag{2}$$

Here, $q = q_\uparrow + q_\downarrow$, $\Delta q = q_\uparrow - q_\downarrow$, $\delta q = q_\top + q_\perp$, x denotes the momentum fraction carried by the quark, and $\{\}$ and $[\]$ denote symmetrization and antisymmetrization respectively. We note that odd moments $\langle x^n \rangle_q$ are obtained from deep inelastic electron or muon scattering structure functions F_1 or F_2 , even moments of $\langle x^n \rangle_{\Delta q}$ are determined from g_1 , and these moments are proportional to the quantities v_{n+1} and a_n defined in ref.[3]. In addition, g_2 also determines the quantity d_n

$$\langle PS | \bar{\psi} \gamma^{[\sigma} \gamma_5 i D^{\{\mu_1} \dots i D^{\mu_n\} \psi | PS \rangle} = \frac{1}{n} d_n S^{[\sigma} P^{\{\mu_1} \dots P^{\mu_n\}} \tag{3}$$

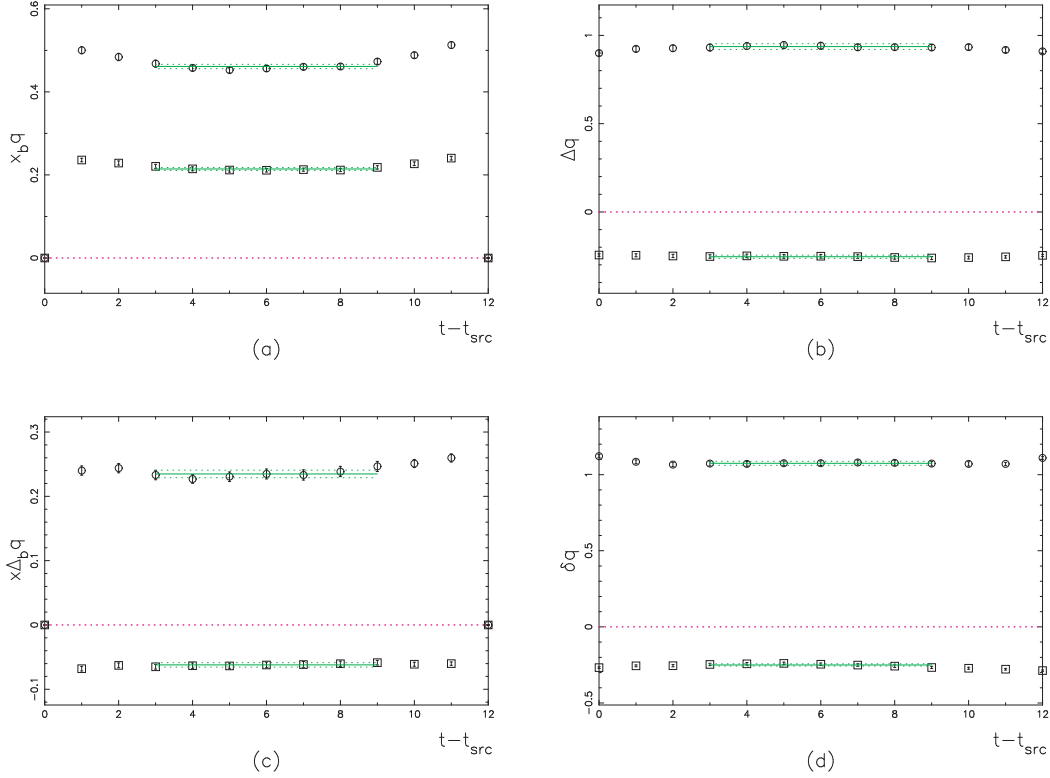


Figure 2. Plateaus in measurements of operators in a zero momentum ground state as a function of the euclidean time separation from the source.

although the lattice calculation of d_n with Wilson fermions is complicated by mixing with the lower dimension operator $\frac{1}{a}\gamma^{[\sigma}\gamma_5\gamma^{\{\mu_1}\dots iD^{\mu_n\}}$.

Even moments $\langle x^n \rangle_q$ are obtained from deep inelastic neutrino scattering, and in addition, a variety of other processes have contributed to what is now a detailed empirical knowledge of the quark and antiquark distributions in the nucleon. We will subsequently compare our results with moments calculated from the CTEQ, MRS, and GRV global fits to the world supply of data.

3. CALCULATION OF MATRIX ELEMENTS

Proton matrix elements of the operators in Eq.2 are calculated by evaluating the connected and disconnected diagrams shown in Fig. 1. Note that both the connected and disconnected diagrams each receive contributions from quarks and antiquarks. Depending on the moment, by Eq.1, the sum of the diagrams yields either the sum or difference of the moments of the quark and antiquark distributions. Because it is technically much more difficult to evaluate the disconnected diagrams, our present calculations only include connected diagrams. Fortunately, the disconnected diagrams are flavor independent, so they cancel out of the flavor non-singlet difference between up and down quark distributions. Hence, in Table 3, we compare lattice calculation of the difference between connected diagrams for up and down quarks with the corresponding difference of moments of experimental data for the sum or difference of quark and antiquark distributions.

On the lattice, connected diagrams are evaluated by calculating a three point function

Table 1
Lattice Operators

	H(4) mix	\vec{p}	lattice operator
$\langle x \rangle_q^{(a)}$	6_3^+	no	$\neq 0$ $\bar{q}\gamma_{\{1}\overleftrightarrow{D}_4\}q$
$\langle x \rangle_q^{(b)}$	3_1^+	no	0 $\bar{q}\gamma_4\overleftrightarrow{D}_4q - \frac{1}{3}\sum_{i=1}^3\bar{q}\gamma_i\overleftrightarrow{D}_i q$
$\langle x^2 \rangle_q$	8_1^-	yes	$\neq 0$ $\bar{q}\gamma_{\{1}\overleftrightarrow{D}_1\overleftrightarrow{D}_4\}q - \frac{1}{2}\sum_{i=2}^3\bar{q}\gamma_{\{i}\overleftrightarrow{D}_i\overleftrightarrow{D}_4\}q$
$\langle x^3 \rangle_q$	2_1^+	no*	$\neq 0$ $\bar{q}\gamma_{\{1}\overleftrightarrow{D}_1\overleftrightarrow{D}_4\overleftrightarrow{D}_4\}q + \bar{q}\gamma_{\{2}\overleftrightarrow{D}_2\overleftrightarrow{D}_3\overleftrightarrow{D}_3\}q - (3 \leftrightarrow 4)$
$\langle 1 \rangle_{\Delta q}$	4_4^+	no	0 $\bar{q}\gamma^5\gamma_3q$
$\langle x \rangle_{\Delta q}^{(a)}$	6_3^-	no	$\neq 0$ $\bar{q}\gamma^5\gamma_{\{1}\overleftrightarrow{D}_3\}q$
$\langle x \rangle_{\Delta q}^{(b)}$	6_3^-	no	0 $\bar{q}\gamma^5\gamma_{\{3}\overleftrightarrow{D}_4\}q$
$\langle x^2 \rangle_{\Delta q}$	4_2^+	no	$\neq 0$ $\bar{q}\gamma^5\gamma_{\{1}\overleftrightarrow{D}_3\overleftrightarrow{D}_4\}q$
$\langle 1 \rangle_{\delta q}$	6_1^+	no	0 $\bar{q}\gamma^5\sigma_{34}q$
$\langle x \rangle_{\delta q}$	8_1^-	no	$\neq 0$ $\bar{q}\gamma^5\sigma_{3\{4}\overleftrightarrow{D}_1\}q$
d_1	6_1^+	no**	0 $\bar{q}\gamma^5\gamma_{[3}\overleftrightarrow{D}_4]q$
d_2	8_1^-	no**	$\neq 0$ $\bar{q}\gamma^5\gamma_{[1}\overleftrightarrow{D}_{\{3}\overleftrightarrow{D}_4\}q$

in which a source creates a state with the quantum numbers of the proton, the operator acts on this state, and a sink finally annihilates the state. Because evolution in imaginary time filters out the ground state, when the operator is sufficiently far from both the source and sink, it acts in the ground state and produces the desired ground state matrix element. As the time at which it acts approaches either the source or sink, it sees excited state contaminants, yielding a central plateau corresponding to the physical matrix element and exponential contaminants at the edges. Obviously, it is beneficial to optimize the overlap of the source with the ground state to maximize the plateau region and minimize the effect of the excited state contaminants at the edges.

In this work, connected diagrams were calculated using sequential propagators generated by the upper two components of the nucleon source $J^\alpha = u_a^\alpha u_b^\beta (C\gamma_5)_{\beta,\beta'} d_c^{\beta'} \epsilon^{abc}$. The overlap with the physical proton ground state was optimized using Wuppertal smearing [4] to maximize the overlap $P(0) = |\langle J|0\rangle|^2$. Varying the smearing reduced P by over 4 orders of magnitude, yielding an overlap with the physical ground state of approximately 50%. Dirichlet boundary conditions were used for quarks in the t-direction.

The resulting plateaus for four operators that could be measured in a proton with zero three-momentum are shown in Fig. 2. Here one observes both a statistically well determined central plateau region and the effectiveness with which the excited state contaminants have been reduced by the optimized source.

4. OPERATORS AND PERTURBATIVE RENORMALIZATION

The continuum operators defined above are approximated on a discrete cartesian lattice using representations of the hypercubic group that have been chosen to eliminate operator mixing as much as possible and to minimize the number of non-zero components of the nucleon momentum. The operators we have used are shown in Table 1, where we have

Table 2

Perturbative renormalization

	γ	B^{LATT}	$B^{\overline{MS}}$	$Z_{\beta=6.0}$	$Z_{\beta=5.6}$
$\langle x \rangle_q^{(a)}$	$\frac{8}{3}$	-3.16486	$-\frac{40}{9}$	0.989	0.988
$\langle x \rangle_q^{(b)}$	$\frac{8}{3}$	-1.88259	$-\frac{40}{9}$	0.978	0.977
$\langle x^2 \rangle_q$	$\frac{23}{6}$	-19.57184	$-\frac{67}{9}$	1.102	1.110
$\langle x^3 \rangle_q$	$\frac{157}{30}$	-35.35192	$-\frac{2216}{225}$	1.215	1.231
$\langle 1 \rangle_{\Delta q}$	0	15.79628	0	0.867	0.857
$\langle x \rangle_{\Delta q}^{(a)}$	$\frac{8}{3}$	-4.09933	$-\frac{40}{9}$	0.997	0.997
$\langle x \rangle_{\Delta q}^{(b)}$	$\frac{8}{3}$	-4.09933	$-\frac{40}{9}$	0.997	0.997
$\langle x^2 \rangle_{\Delta q}$	$\frac{23}{6}$	-19.56159	$-\frac{67}{9}$	1.102	1.110
$\langle 1 \rangle_{\delta q}$	1	16.01808	-1	0.856	0.846
$\langle x \rangle_{\delta q}$	3	-4.47754	-5	0.996	0.995
d_1	0	0.36500	0	0.997	0.997
d_2	$\frac{7}{6}$	-15.67745	$-\frac{35}{18}$	1.116	1.124

indicated whether the spatial momentum components are non-zero and whether mixing occurs. Note, no* indicates a case in which mixing could exist in general but vanishes perturbatively for Wilson or overlap fermions and no** indicates perturbative mixing with *lower* dimension operators for Wilson fermions but no mixing for overlap fermions. Because the statistical errors are much larger for sources projected to non-zero momentum, the moments corresponding to operators requiring non-zero momentum are presently not well determined.

To convert from lattice regularization at the scale of the inverse lattice spacing $1/a$ to the continuum \overline{MS} scheme at momentum scale Q , we use the one-loop perturbation theory result

$$O_i^{\overline{MS}}(Q^2) = \sum_j \left(\delta_{ij} + \frac{g_0^2}{16\pi^2} \frac{N_c^2 - 1}{2N_c} \left(\gamma_{ij}^{\overline{MS}} \log(Q^2 a^2) - (B_{ij}^{LATT} - B_{ij}^{\overline{MS}}) \right) \right) \cdot O_j^{LATT}(a^2).$$

The anomalous dimensions γ_{ij} and the finite constants B_{ij} we have calculated and used in this work are tabulated in Table 2 [5].

5. RESULTS

The moments listed in Table 1 were calculated [1,2] on $16^3 \times 32$ lattices for Wilson fermions in full QCD at $\beta = 5.6$ using 200 SESAM configurations at each of 4 κ 's and at $\beta = 5.5$ using 100 SCRI configurations at 3 κ 's. They were also calculated with two sets of 100 full QCD configurations cooled with 50 cooling steps and in quenched QCD at $\beta = 6.0$ using 200 configurations at each of 3 κ 's. Typical linear chiral extrapolations for operators calculated with nucleon momentum equal to zero are shown in Figure 3 for full and quenched calculations of $\langle x \rangle_q$ and $\langle x \rangle_{\Delta q}$, showing agreement within statistical errors. To avoid finite volume errors at the lightest quark mass, the SESAM [6] results were extrapolated using the three heaviest quark masses. Table 3 shows a major result of

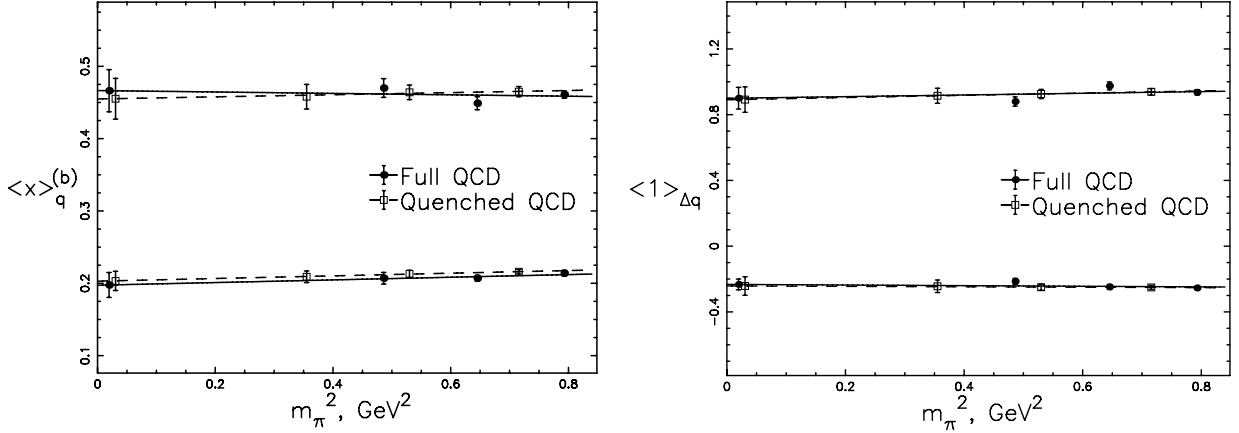


Figure 3. Comparison of linear chiral extrapolations of full and quenched calculations of $\langle x \rangle_q^{(b)}$ and $\langle 1 \rangle_{\Delta q}$ showing agreement within statistical errors

our work, that there is complete agreement within statistics between full and quenched results. Statistics with the SCRI configurations [7] are currently being increased to study the dependence on the coupling constant.

Typical chiral extrapolations for cooled configurations are compared with the corresponding uncooled full QCD calculations in Figure 4. This qualitative agreement between cooled and uncooled results occurs at light quark mass for all the twist-2 matrix elements we calculated and demonstrates the degree to which the instanton content of the configurations and their associated zero modes dominate light hadron structure [8].

A major crisis and longstanding puzzle in this field has been the fact that when quenched lattice results are linearly extrapolated in m_q , results disagree with experiment at the 20-50% level. Our results clearly show that inclusion of quark-antiquark excitation from the Dirac Sea does not resolve this discrepancy. Salient examples from Table 3 are $\langle x \rangle_{u-d} \sim 0.25 - 0.27$ compared with the experimental result 0.15 and $g_A = \langle 1 \rangle_{\Delta u-\Delta d} \sim 1.0 - 1.1$ compared with the experimental result 1.26.

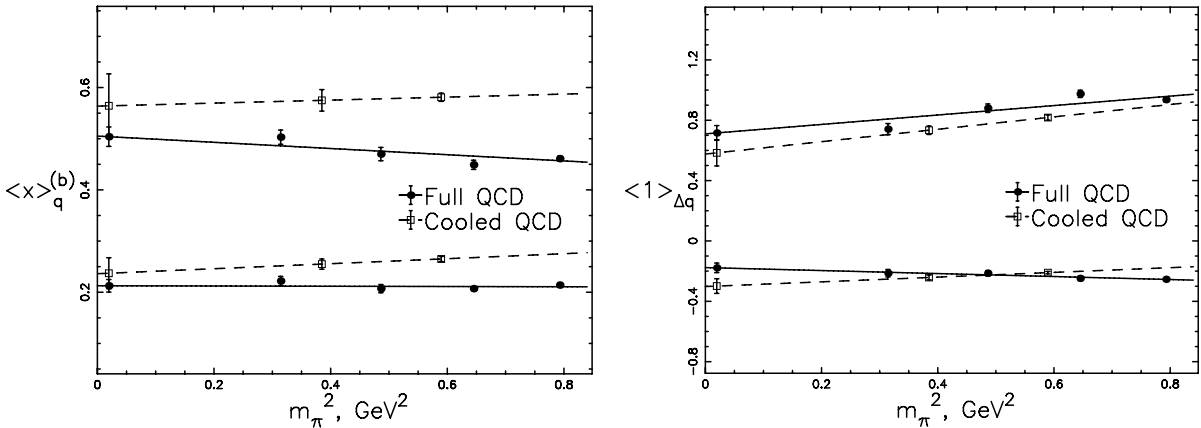


Figure 4. Comparison of linear chiral extrapolations of full and cooled calculations of $\langle x \rangle_q^{(b)}$ and $\langle 1 \rangle_{\Delta q}$ showing the extent to which instantons reproduce the full result.

Table 3

Comparison of linear extrapolations of our full QCD and quenched results with other lattice calculations and phenomenology at 4 GeV in \overline{MS}

Conn. M. E.	QCDSF	QCDSF ($a = 0$)	SESAM	Quenched	Full QCD (3 pts)	Phen. ($q \pm \bar{q}$)
$\langle x \rangle_u$	0.452(26)			0.454(29)	0.459(29)	
$\langle x \rangle_d$	0.189(12)			0.203(14)	0.190(17)	
$\langle x \rangle_{u-d}$	0.263(17)			0.251(18)	0.269(23)	0.154(3)
$\langle x^2 \rangle_u$	0.104(20)			0.119(61)	0.176(63)	
$\langle x^2 \rangle_d$	0.037(10)			0.029(32)	0.031(30)	
$\langle x^2 \rangle_{u-d}$	0.067(22)			0.090(68)	0.145(69)	0.055(1)
$\langle x^3 \rangle_u$	0.022(11)			0.037(36)	0.069(39)	
$\langle x^3 \rangle_d$	-0.001(7)			0.009(18)	-0.010(15)	
$\langle x^3 \rangle_{u-d}$	0.023(13)			0.028(49)	0.078(41)	0.023(1)
$\langle 1 \rangle_{\Delta u}$	0.830(70)	0.889(29)	0.816(20)	0.888(80)	0.860(69)	
$\langle 1 \rangle_{\Delta d}$	-0.244(22)	-0.236(27)	-0.237(9)	-0.241(58)	-0.171(43)	
$\langle 1 \rangle_{\Delta u-\Delta d}$	1.074(90)	1.14(3)	1.053(27)	1.129(98)	1.031(81)	1.248(2)
$\langle x \rangle_{\Delta u}$	0.198(8)			0.215(25)	0.242(22)	
$\langle x \rangle_{\Delta d}$	-0.048(3)			-0.054(16)	-0.029(13)	
$\langle x \rangle_{\Delta u-\Delta d}$	0.246(9)			0.269(29)	0.271(25)	0.196(9)
$\langle x^2 \rangle_{\Delta u}$	0.04(2)			0.027(60)	0.116(42)	
$\langle x^2 \rangle_{\Delta d}$	-0.012(6)			-0.003(25)	0.001(25)	
$\langle x^2 \rangle_{\Delta u-\Delta d}$	0.05(2)			0.030(65)	0.115(49)	0.061(6)
δu_c	0.93(3)	0.980(30)		1.01(8)	0.963(59)	
δd_c	-0.20(2)	-0.234(17)		-0.20(5)	-0.202(36)	
d_2^u	-0.206(18)			-0.233(86)	-0.228(81)	
d_2^d	-0.035(6)			0.040(31)	0.077(31)	

A breakthrough in resolving this crisis has been the understanding that the physical origin of these discrepancies is the inadequate treatment of the pion cloud in the nucleon that has been necessary because of limited computational resources. By necessity, present calculations are restricted to quark masses that are so heavy that the pion mass is above 600 MeV and the pion cloud surrounding the nucleon is strongly suppressed. Physical quantities like the nucleon magnetic moment and axial charge clearly depend strongly on the pion current, and should therefore be very sensitive to the absence of the full pion cloud. Furthermore, because of the rapid, nonlinear variation from the chiral logs arising from Goldstone boson loops, it is clear that a linear extrapolation is completely inadequate to describe the correct chiral physics.

In a recent work[10], we have shown that chiral extrapolation incorporating the leading non-analytic behavior from chiral perturbation theory can systematically resolve the discrepancies in the moments $\langle x^n \rangle_{u-d}$ using the formula:

$$\langle x^n \rangle_u - \langle x^n \rangle_d \sim a_n \left[1 - \frac{(3g_A^2 + 1)m_\pi^2}{(4\pi f_\pi)^2} \ln\left(\frac{m_\pi^2}{m_\pi^2 + \mu^2}\right) \right] + b_n m_\pi^2 \quad (4)$$

The coefficient of the leading non-analytic behavior $m_\pi^2 \ln(m_\pi^2)$ is determined from chiral perturbation theory. The parameter μ specifies the scale above which pion loops no longer

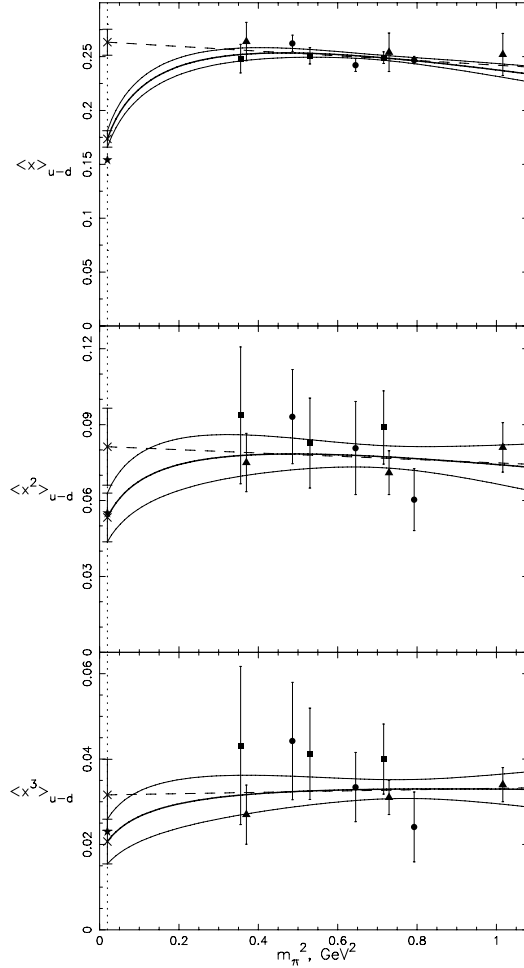


Figure 5. Chiral extrapolation of $\langle x \rangle_q^{(b)}$, $\langle x^2 \rangle_q$, and $\langle x^3 \rangle_q$ using Eq. 4

produce rapid variation. It corresponds to the upper limit of the momentum integration generated physically by the inverse size of the quark core of the nucleon that serves as the source for the pion field. As shown in Fig. 5, the value $\mu \sim 550$ MeV from ref [10], which is consistent with the value required to extrapolate the nucleon magnetic moment and with chiral nucleon models, extrapolates the world's supply of lattice data to the experimental values of $\langle x \rangle_{u-d}$, $\langle x^2 \rangle_{u-d}$, and $\langle x^3 \rangle_{u-d}$. From this figure, it is also clear that 5% measurements down to $m_\pi^2 = 0.05$ GeV^2 , requiring a spatial volume of order $(4.3 \text{ fm})^3$, would provide data for a definitive lattice calculation. From the known scaling of present hybrid Monte Carlo algorithms, this calculation will require 8 Teraflops-years and thus can be carried out on the next generation of 10-Teraflops computers.

FUTURE PROMISE

With the present tools of lattice field theory and the physical understanding of the essential role of the pion cloud, we now have the framework for definitive calculation of hadron structure. Improved actions will allow a reliable extrapolation to the continuum

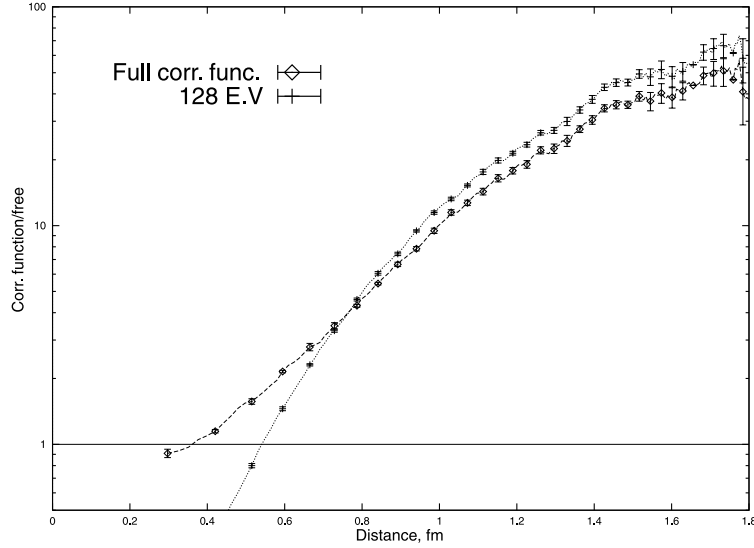


Figure 6. Graph showing how the propagation of a pion in the QCD vacuum (diamonds) is well approximated by a propagator containing only the lowest 128 eigenmodes

limit. Chiral fermions now implement an exact chiral symmetry on the lattice. Partially quenched chiral perturbation theory provides a systematic framework to measure the relevant parameters of effective field theory for unambiguous chiral extrapolation using optimal combinations of valence and sea quark masses, including corrections for finite volume and fixed topology. As explained above, computers providing sustained performance of tens of Teraflops will enable calculation in the chiral regime of sufficiently low quark mass and sufficiently large volume for reliable chiral perturbation theory extrapolation. Renormalization coefficients and mixing parameters can now be calculated nonperturbatively. And finally, eigenmode expansion techniques [8,11] using the dominance of propagators by low eigenmodes as illustrated in Fig. 6 enable the calculation of previously intractable disconnected diagrams.

In conclusion, understanding the quark and gluon structure of QCD requires not only frontier facilities for experimental measurements, but also frontier facilities for fundamental lattice calculations. The time has come to think of dedicated computers in the same way as one thinks of experimental apparatus for the field. And, as has been so effective in experimental physics, the time has also come for international collaboration in large scale computation.

ACKNOWLEDGMENTS

It is a pleasure to acknowledge the contributions of D. Dolgov, S. Capitani, D. Renner, A. Pochinsky, and R. Brower, to these lattice calculations, P. Dreher to the computer cluster infrastructure, N. Eicker, T. Lippert, and K. Schilling in providing the SESAM configurations, R. G. Edwards, and U. M. Heller in providing the SCRI configurations, and W. Detmold, W. Melnitchouk, and A. W. Thomas in understanding the chiral extrapolation.

REFERENCES

1. D. Dolgov, Ph.D. dissertation, MIT (2000).
2. D. Dolgov, R. Brower, S. Capitani, P. Dreher, J. W. Negele, A. Pochinsky, D. B. Renner, N. Eicker, Th. Lippert, K. Schilling, R. G. Edwards, U. M. Heller, Phys. Rev. D in press, arXiv:hep-lat/0201021.
3. M. Göckeler *et al.*, Phys. Rev. D53 (1996) 2317; Phys. Lett. B414 (1997) 340; hep-ph/9711245; hep-ph/9909253; C. Best *et al.*, hep-ph/9706502; S. Capitani *et al.*, Nucl. Phys. (Proc. Suppl.) B79 (1999) 548.
4. C. Alexandrou *et al.*, Phys. Lett. B256 (1991) 60; C. R. Allton *et al.*, Phys. Rev. D47 (1993) 5128.
5. S. Capitani and G. Rossi, Nucl. Phys. B433 (1995) 351; G. Beccarini *et al.*, Nucl. Phys. B456 (1995) 271; M. Göckeler *et al.* Nucl. Phys. B472 (1996) 309; S. Capitani *et al.*, hep-lat/0007004; S. Capitani, hep-lat/0005008; hep-lat/0009018.
6. N. Eicker *et al.*, Phys. Rev. D59 (1999) 014509; S. Güsken *et al.*, Phys. Rev. D59 (1999) 054504; hep-lat/9901009.
7. K. M. Bitar *et al.* Phys. Rev. D54, (1996) 3546.
8. M. -C. Chu *et al.*, Phys. Rev. D49 (1994) 6039; T. L. Ivanenko and J. W. Negele, Nucl. Phys. (Proc. Suppl.) B63 (1998) 504; D. Dolgov *et al.*, Nucl. Phys. (Proc. Suppl.) B73 (1999) 300.
9. T. Gehrmann and W. J. Stirling, Phys. Rev. D53 (1996) 6100.
10. W. Detmold, W. Melnitchouk, J. W. Negele, D. B. Renner and A. W. Thomas, Phys. Rev. Lett. **87**, 172001 (2001) [arXiv:hep-lat/0103006].
11. H. Neff, N. Eicker, T. Lippert, J. W. Negele and K. Schilling, “On the low fermionic eigenmode dominance in QCD on the lattice,” Phys. Rev. D **64**, 114509 (2001) [arXiv:hep-lat/0106016].